3-D Printed *W*-Band Waveguide Twist With Integrated Filtering

Liyan Zhu, Ian W. Rossuck, Roshan Payapulli, Sang-Hee Shin, *Member, IEEE*, and Stepan Lucyszyn, *Fellow, IEEE*

***Abstract*— This work demonstrates the integration of a low-pass filter into a 90° waveguide twist at *W*-band (75–110 GHz), manufactured using polymer-based 3-D printing. For the first time, a 1-D periodic electromagnetic bandgap (EBG) structure is incorporated within a waveguide twist. Unlike conventional filters, implemented using irises and septa, EBG structures employing hollow cavities are structurally robust and mechanically insensitive to 3-D printing. The measured average passband insertion loss is only 0.48 dB at the *W*-band while using our unconventional split-block solution (*H*-plane *a*-edge split with raised lips). A nontwist thru filter has also been demonstrated, as a reference. Our approach demonstrates the potential for the low-cost manufacture of compact and high-performance multifunctional integrated waveguide components at millimeter-wave frequencies.**

***Index Terms*— 3-D printing, additive manufacturing, electromagnetic bandgap (EBG), millimeter wave (mm-wave), rectangular waveguide, *W*-band, waveguide filter, waveguide twist, WR-10.**

I. Introduction

ADDITIVE manufacturing using polymer-based 3-D printing is considered as an emerging technology for its design flexibility, fast iterative fabrication, lightweight, and low cost. Since 2015, this technology has demonstrated its potentials for applications in metal-pipe rectangular waveguide (MPRWG) components for use across the microwave-to-terahertz (THz) frequency spectrum: at *X*-band (8–12 GHz) [1]; *W*-band (75–110 GHz) [1]; *D*-band (110–170 GHz) [2]; *G*-band (140–220 GHz) [3]; WM-570 band (325–500 GHz) [4]; and WM-380 band (500–750 GHz) and WM-250 band (750 GHz–1.1 THz) [5].

In modern communications, radar, and sensor systems, waveguide twists and filters are both important passive components, providing respective polarization rotation and frequency selection functionalities, which are normally separate. Compared to the conventional approach of cascading these individual components, integration is more attractive because of its miniaturization, lightweight, and low-loss properties. To date, a number of integrated twist-filter waveguide components have been reported in the open literature. For example, some use gradual rotation [6], [7], [8], while another employs a step-twist transition [9]. Diaphragm irises [6], [9], transverse offset irises [7], and *E*-plane septum insert [8] are used to realize the corresponding filter responses.

Rotational irises and septa represent the most common approach to realize a twist filter. However, irises and septa become more structurally delicate and sensitive as the working frequency is increased, requiring more accurate manufacturing techniques—not suitable for 3-D printing.

An alternative method to provide frequency selection is the use of 1-D electromagnetic bandgap (EBG) structures. An EBG structure is a class of periodic metamaterial with unique properties that prevent wave propagation (stop bands) at certain frequencies. EBG structures are commonly used in gap waveguides to stop leakage from the air gap, without the need for electrical contact between the top and bottom waveguide parts. These periodic structures can employ different unit cell implementations, including mushroom [10], metal pin [11], [12], [13], and hollow cavity [14], [15] solutions. Mushroom-EBG structures are normally integrated into printed circuit boards, which are inherently more lossy than the fully metal-based solutions, due to dielectric losses. For the two metal-based pin and cavity solutions, the latter is structurally more robust and can be more cost-effective, when compared to the former. As a result, this approach is adopted here for low-cost and high-performance applications at millimeter-wave (mm-wave) frequencies.

After an exhaustive literature search, to the best of our knowledge, we demonstrate the first proof of principle for a 90° waveguide twist with integrated EBG filter. Note that the previously reported waveguide twist-filter examples have either bandpass filter (BPF) or low-pass filter (LPF) passbands within the frequency range between 10 and 33 GHz. In this letter, we also provide a low-cost manufacturing solution, using 3-D printing, which demonstrates high performance with a passband between 75 and 92.6 GHz.

II. Filter Design

With reference to Fig. 1 and [15], the number of unit cells *N* determines the filter's stopband rejection roll-off characteristic. Increasing the number of unit cells can provide better rejection at the expense of an increase in passband insertion loss. The air gap *g* controls the interaction between the top and bottom

Manuscript received 13 December 2022; revised 25 January 2023 and 6 February 2023; accepted 20 February 2023. Date of publication 2 March 2023; date of current version 7 June 2023. This work was supported by the U.K. Space Agency's Centre for Earth Observation Instrumentation (CEOI), under Grant RP10G0435A202. *(Corresponding author: Stepan Lucyszyn.)*

Liyan Zhu, Ian W. Rossuck, Roshan Payapulli, and Stepan Lucyszyn are with the Department of Electrical and Electronic Engineering, Imperial College London, SW7 2AZ London, U.K. (e-mail: liyan.zhu19@imperial.ac.uk; ian.rossuck15@imperial.ac.uk; roshan.payapulli14@imperial.ac.uk; s.lucyszyn@imperial.ac.uk).

Sang-Hee Shin is with the Department of Electromagnetic and Electrochemical Technologies, National Physical Laboratory, TW11 0LW Teddington, U.K. (e-mail: sang-hee.shin@npl.co.uk).

Color versions of one or more figures in this letter are available at https://doi.org/10.1109/LMWT.2023.3247942.

Digital Object Identifier 10.1109/LMWT.2023.3247942

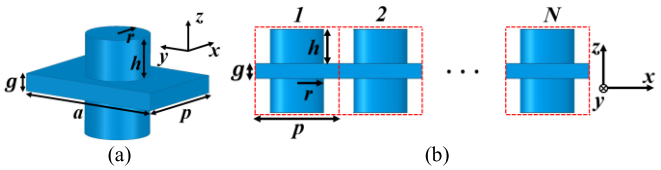

Fig. 1. Periodic mirror-symmetric hollow structure and its unit cell. (a) Unit cell. (b) 1-D periodic structure containing N unit cells.

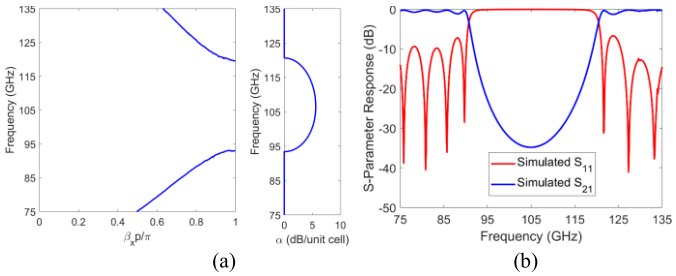

Fig. 2. HFSS simulations. (a) Dispersion diagrams for the unit cell (left) phase constant β_x and (right) attenuation per unit cell α. (b) Eight cells cascaded.

EBG units and, therefore, g should be small enough so that the effects of EBG units are observable. However, a small gap between the top and bottom parts can cause strong reflections and, therefore, poor return loss responses. Therefore, $g = 0.30$ mm is chosen as a compromise when considering both effects. The unit cell periodicity p corresponds to half the guide wavelength at the mid-stopband frequency. Increasing the periodicity can narrow the stopband region. Increasing the unit cell height h provides better rejection within the stopband. Above $h = 0.60$ mm, the filter responses effectively remain unchanged. Here, $h = 0.70$ mm is chosen to compensate for fabrication errors. The increase of the radius r provides a denser unit cell distribution, and the rejection ability within the stopband is, therefore, improved.

Fig. 1(a) and (b) shows the unit cell of a mirror-symmetric hollow structure and the 1-D periodic structure with N unit cells along the propagating x-axis, respectively. The physical dimensions for the unit cell are: $a = 2.54$ mm, $g = 0.30$ mm, $p = 1.70$ mm, $h = 0.70$ mm, and $r = 0.55$ mm.

All electromagnetic (EM) full-wave simulations are undertaken using Ansys High-Frequency Structure Simulator (HFSS), with bulk copper. Fig. 2(a) and (b) shows the dispersion diagram for the designed unit cell and eight identical unit cells cascaded together, respectively. These are obtained using the HFSS eigenmode solver and a standard Bloch analysis [16]. It can be seen that the lower waveguide EBG cutoff frequency for the first propagation mode is 64.1 GHz, which is higher than the 59.0-GHz cutoff frequency for the waveguide's TE_{10} mode of propagation. The stopband is from 93.3 to 121.1 GHz, with a peak attenuation of 5.6 dB/unit cell at 106.8 GHz; both filters are designed to have a 3-dB cutoff frequency of 93 GHz.

Both EBG filters are designed to be compatible with standard WR-10 MPRWGs, having internal height and width cross-sectional aperture dimensions $a = 2540$ μm and $b = 1270$ μm, respectively. A split-block design is chosen, with "trough-and-lid" assembly, as this ensures the removal of

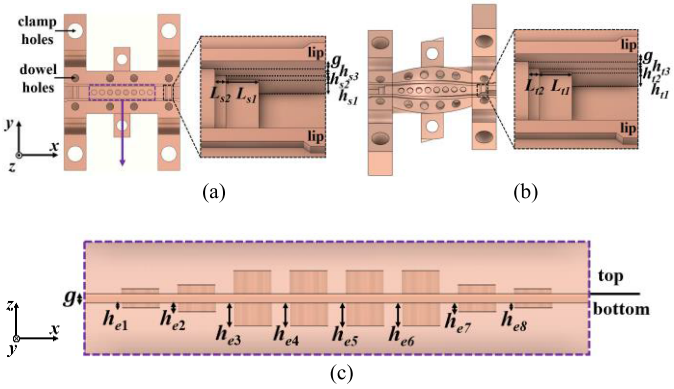

Fig. 3. EBG filter design integrated into a waveguide. (a) Plan view of thru. (b) Plan view of twist. (c) Side view of thru showing the hollow cavities.

all resin residues after 3-D printing and allows the waveguide's internal walls to be sufficiently metallized [2], [3].

Fig. 3(a) and (b) shows the plan views for the bottom parts of the designed filters. Clamp holes are designed for screw tightening and dowel holes are used for alignment. A close-in view of the thru filter's step transition is shown in Fig. 3(a), where the physical dimensions are: $L_{s1} = 0.90$ mm, $L_{s2} = 0.30$ mm, $h_{s1} = 0.55$ mm, $h_{s2} = 0.15$ mm, and $h_{s3} = 0.27$ mm. The step transition effectively reduces the waveguide's height from b down to g. The raised lips are designed to provide good ohmic contact between the bottom and the top parts, used to mitigate against EM energy leakage. Lip widths on both edges of the flanges are broadened to provide enhanced structural tolerances when the top and bottom parts are assembled [2], [3]. Fig. 3(c) shows the side view for the mirror-symmetric hollow cavities of the thru filter. Simulations show that the heights for the first and last two cavities have significant effects on the impedance matching and, therefore, they are reduced to form a discrete taper that minimizes reflections. The physical dimensions for the designed mirror-symmetric structure are: $g = 0.30$ mm, $h_{e1} = h_{e8} = 0.15$ mm, $h_{e2} = h_{e7} = 0.27$ mm, and $h_{e3} = h_{e4} = h_{e5} = h_{e6} = 0.70$ mm.

Our W-band 90° twist has a flange-to-flange component length of 24.60 mm, which includes 4.65-mm thru lines within each flange. This gives a total twist length of $2.354\lambda_{gL}$, where $\lambda_{gL} = 6.50$ mm is the guided wavelength at the lower band-edge frequency of 75 GHz (giving the worst case attenuation), having a rotational smoothness of $38°/\lambda_{gL}$.

To transform from a waveguide thru to a twist, a smooth rotation is formed to realize the final 90° polarization shift, as shown in Fig. 3(b). The mirror-symmetric hollow structure design is exactly the same as the one shown in Fig. 3(c), except for the physical rotation of 10° between adjacent cavities. The transition design, shown in Fig. 3(b), is adjusted to accommodate for the rotation. The physical dimensions for the designed step transition are: $L_{t1} = 0.85$ mm, $L_{t2} = 0.30$ mm, $h_{t1} = 0.50$ mm, $h_{t2} = 0.17$ mm, and $h_{t3} = 0.30$ mm.

III. Fabrication

The 3-D printing technology used in this work is low-cost masked stereolithography apparatus (MSLA). The Elegoo

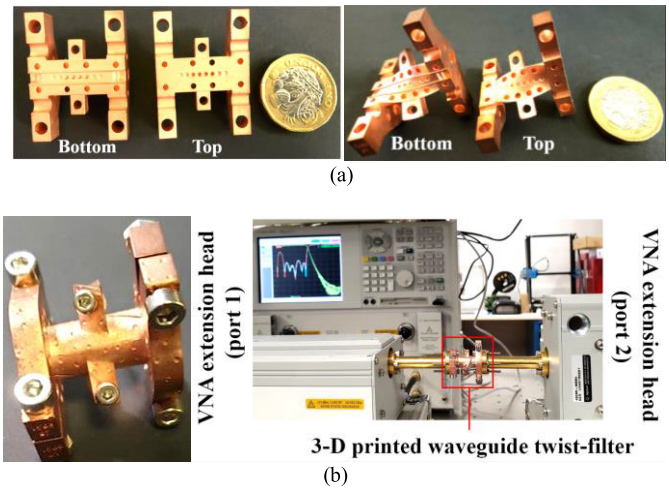

Fig. 4. Photographs of the filters. (a) Disassembled thru (left) and twist (right). (b) Assembled twist filter and its measurement setup.

water washable photopolymer resin (Ceramic Gray) was used; mainly for its low shrinkage, ease of postprocessing, and low odor. Our Phrozen Sonic Mini 8K MSLA 3-D printer has a quoted 22-μm pixel resolution in the x–y build plane and the layer thickness in the z-direction is set to be 20 μm. The printing orientations for our filters are important. The thru filter is placed horizontally on the build plate, while the twist filter is rotated by 45° to ensure the symmetric printing for both ports. The 3-D printed parts are initially electroless plated with a thin layer of nickel and then electroplated with a 25-μm layer of copper, which is compensated for in our simulations. This level of thickness is required to ensure that all edges and the bottom of the cylinders are sufficiently plated. We previously determined [2] that the average radius of hemispherical protrusions is 3.7 μm, having an average separation distance of 17 μm, giving an rms profile roughness of $R_q = 1.41$ μm.

IV. Measured Results

Measurements were made at Imperial College London, London, U.K., using the Agilent Technologies E8361A PNA vector network analyzer and 67–110-GHz frequency extension heads. Fig. 4(a) and (b) shows the disassembled 3-D printed filters and the assembled twist filter and its W-band test setup, respectively.

The simulation and measurement results for the thru filter and twist filter are shown in Fig. 5(a) and (b), respectively. Good agreement between the simulation and measurement results is achieved. The measured ripples are relatively very small and due to Fabry–Perot resonances caused by impedance mismatches at both measurement ports. For the thru filter, the measured 3-dB cutoff frequency is 90.5 GHz and the average passband insertion loss is 0.87 dB at the W-band. In the rejection band, the attenuation is greater than 20 dB above 93.1 GHz, where the peak attenuation of 46.1 dB is achieved at 107.7 GHz.

For the twist filter, the measured 3-dB cutoff frequency is 92.6 GHz and the average insertion loss is only 0.48 dB. In the rejection band, the attenuation is greater than 20 dB above 95.8 GHz, where the peak attenuation of 43.3 dB is

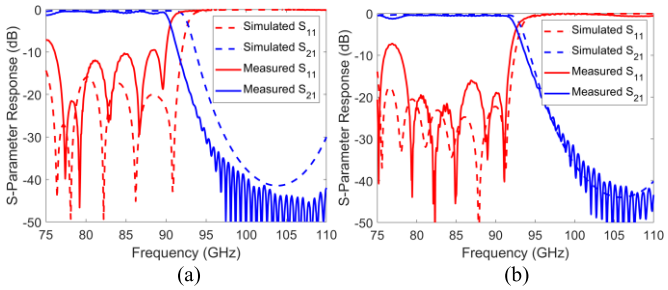

Fig. 5. Simulated and measured results. (a) Thru filter. (b) Twist filter.

TABLE I
Comparison Summary of Integrated Twist Filters

Band	Passband (GHz)	Filter Type	Functions	Return Loss (dB)	Insertion Loss (dB)	Year [Ref.]
X	10.6-11.0	E-plane Septum	Twist, BPF	≥ 18	0.44 worst	2021 [8]
Ku	14.7-15.3	Diaphragm Irises	Twist, BPF, Bend	≥ 13	0.85 average	2022 [6]
Ku	12.0-16.2	Offset Irises	Twist, LPF, Bend	≥ 20	0.20 worst	2018 [7]
Ka	31.4-32.4	Diaphragm Irises	Twist, BPF	≥ 15	0.84 average	2020 [9]
W	75.0-92.6	EBG	Twist, LPF	≥ 8	1.27 worst 0.48 average	2023 **This work**

achieved at 107.9 GHz. According to the attenuation per unit cell given in Fig. 2(b), with both filters employing eight unit cells, the predicted peak attenuation is 44.8 dB. This is in good agreement with our measured values of 46.1 and 43.3 dB for the thru filter and twist filter, respectively.

A literature review has been undertaken of integrated twist-filter waveguide components and a comparison summary is given in Table I. As shown in Table I, only one previously reported example could be found at mm-wave frequencies [10].

V. Conclusion

In this letter, a new mm-wave multifunctional integrated waveguide component has been demonstrated. For the first time, a 1-D periodic EBG mirror-symmetric hollow structure is incorporated within a waveguide thru and twist to implement target LPF responses at the W-band. The measured twist filter meets its 93-GHz target cutoff frequency and its average passband insertion loss is only 0.48 dB. The measured thru-filter response, while also being low loss, has a 2-GHz reduction in its cutoff frequency that is believed to be due to random quantization errors in the MSLA printing [3]. Our 1-D periodic metamaterial solution is structurally robust and mechanically insensitive and, as a result, suitable for low-cost manufacture (e.g., using polymer-based 3-D printing), of high mm-wave frequency applications. Multifunctionality reduces the overall component assembly length and eliminates intercomponent flanges, dramatically reducing attenuation; opening up new opportunities for compact, low-loss, and low-cost integrated systems.

References

[1] M. D'Auria et al., "3-D printed metal-pipe rectangular waveguides," *IEEE Trans. Compon., Packag., Manuf. Technol.*, vol. 5, no. 9, pp. 1339–1349, Sep. 2015.

[2] L. Zhu et al., "3-D printed rectangular waveguide 123–129 GHz packaging for commercial CMOS RFICs," *IEEE Microw. Wireless Technol. Lett.*, vol. 33, no. 2, pp. 157–160, Jan. 2023.

[3] L. Zhu, R. Payapulli, S.-H. Shin, M. Stanley, N. M. Ridler, and S. Lucyszyn, "3-D printing quantization predistortion applied to sub-THz chained-function filters," *IEEE Access*, vol. 10, pp. 38944–38963, 2022.

[4] W. J. Otter and S. Lucyszyn, "Hybrid 3-D-printing technology for tunable THz applications," *Proc. IEEE*, vol. 105, no. 4, pp. 756–767, Apr. 2017.

[5] W. J. Otter et al., "3D printed 1.1 THz waveguides," *IET Electron. Lett.*, vol. 53, no. 7, pp. 471–473, Mar. 2017.

[6] Q. Liu, Y. Zhang, F. Zhang, and J. Xu, "A 3D printed waveguide hybrid bandpass filter integrated with twisting and bending functionalities," in *Proc. IEEE Int. Symp. Antennas Propag. USNC-URSI Radio Sci. Meeting (AP-S/URSI)*, Jul. 2022, pp. 2000–2001.

[7] O. A. Peverini et al., "Integration of an H-plane bend, a twist, and a filter in Ku/K-band through additive manufacturing," *IEEE Trans. Microw. Theory Techn.*, vol. 66, no. 5, pp. 2210–2219, May 2018.

[8] C. Bartlett, D. Miek, F. Kamrath, D. Bruhn, and M. Hoft, "X-band 3D-printed metal-insert twist-component for bandpass filter applications," in *IEEE MTT-S Int. Microw. Symp. Dig.*, Nov. 2021, pp. 329–331.

[9] Y. Zhang, F. Zhang, Y. Gao, J. Xu, C. Guo, and X. Shang, "3D printed waveguide step-twist with bandpass filtering functionality," *Electron. Lett.*, vol. 56, no. 11, pp. 527–528, 2020.

[10] E. Pucci, E. Rajo-Iglesias, and P.-S. Kildal, "New microstrip gap waveguide on mushroom-type EBG for packaging of microwave components," *IEEE Microw. Wireless Compon. Lett.*, vol. 22, no. 3, pp. 129–131, Mar. 2012.

[11] A. Tamayo-Dominguez, J.-M. Fernandez-Gonzalez, and M. S. Castaner, "Low-cost millimeter-wave antenna with simultaneous sum and difference patterns for 5G point-to-point communications," *IEEE Commun. Mag.*, vol. 56, no. 7, pp. 28–34, Jul. 2018.

[12] A. Polemi, S. Maci, and P.-S. Kildal, "Dispersion characteristics of a metamaterial-based parallel-plate ridge gap waveguide realized by bed of nails," *IEEE Trans. Antennas Propag.*, vol. 59, no. 3, pp. 904–913, Mar. 2011.

[13] D. Sun and J. Xu, "A novel iris waveguide bandpass filter using air gapped waveguide technology," *IEEE Microw. Wireless Compon. Lett.*, vol. 26, no. 7, pp. 475–477, Jul. 2016.

[14] A. Monje-Real, N. J. G. Fonseca, O. Zetterstrom, E. Pucci, and O. Quevedo-Teruel, "Holey glide-symmetric filters for 5G at millimeter-wave frequencies," *IEEE Microw. Wireless Compon. Lett.*, vol. 30, no. 1, pp. 31–34, Jan. 2020.

[15] Á. Palomares-Caballero, A. Alex-Amor, P. Padilla, and J. F. Valenzuela-Valdés, "Dispersion and filtering properties of rectangular waveguides loaded with holey structures," *IEEE Trans. Microw. Theory Techn.*, vol. 68, no. 12, pp. 5132–5144, Dec. 2020.

[16] M. Bagheriasl, O. Quevedo-Teruel, and G. Valerio, "Bloch analysis of artificial lines and surfaces exhibiting glide symmetry," *IEEE Trans. Microw. Theory Techn.*, vol. 67, no. 7, pp. 2618–2628, Jul. 2019.